SQU Journal For Science, 14 (2009) 25-43

Multiphase Mineral Inclusions in Ferrikaersutite Megacrysts : Implications for Postmagmatic Alteration of the Kaersutite Host

Sobhi Nasir

Department of Earth Sciences, College of Science, Sultan Qaboos University, Email: sobhi@squ.edu.om.

مكتنفات متعددة المعادن في بلورات فريكيروسيتيت خشنة : دلائل على التغيرات الصهرية للكيرسوتيت الحاوي

صبحي نصر

خلاصة: وجدت مكتنفات أولية وثانوية لمعادن متعددة وبدون بقايا للمحاليل ضمن بلورات خشنة من الفريكيروسيتيت ضمن حقل براكين حرات الشام ذات العصر الكينوزوي في سوريا. تحتوي المكتنفات على معادن المجنتيت، والهماتيت، والبسودوبروكيت والبيرويتيت. تم تكوين بلورات الكيرسوتيت من صهير باسانيتي مائي في العمق. تتكون معادن السليكات في المتكنفات من الأوليفين، والبلاجيوكليز، والفلوجوبيت، والهورنبلند، والكلينوبيروكسين والأرثوبيروكسين. تكونت معادن السليكات من الصهير المتداخل والمالئ للكسور والتشققات في معدن الكيرسوتيت. تكون معدن الماجنتيت والبروتيت من خلال التبلور الصهيري والذي تعرض بعد ذلك إلى تغيرات على حرارة منخفضة. أدت التغيرات في المراحل المتأخرة القريبة من السطح الى تكون معادن الهماتيت والليمونيت وكذلك نواج التجوية الدقيقة الحجم والمتكونة من نواتج غنية بالسليكا والحديد، والسليكا والمجنسيوم والألمنيوم، والسليكا والحديد والألمنيوم، والسليكا والألمنيوم ،والسليكا والتيتانيوم والألمنيوم والحديد والكالسيوم. لقد كان تركيب نواتج التجوية محكوما بالتغير المرافق للمرحلة الما بعد صهيرية للكيروسوتيت على حرارة منخفضة من خلال أسطح التشقق والكسور.

ABSTRACT: Primary and secondary multiphase mineral inclusions, without preserved fluid are found in ferrikaersutite megacrysts from the Cenozoic Harrat Ash Sham Volcanic Field in Syria. Mineral phases in the inclusions are magnetite, hematite, pseudobrookite and pyrrhotite. The kaersutite megacrysts formed from a hydrous basanitic melt at depth. Silicate minerals in the inclusions are olivine, plagioclase, phlogopite, hornblende, clino- and orthopyroxene. These silicate minerals crystallized from melt penetration and infillings of veins and fractures in the kaersutite. Magnetite and pyrrhotite inclusion formed through magmatic crystallization which was followed by low temperature alteration and re-equilibration. Late stage near-surface alteration resulted in the formation of hematite, limonite and fine-grained weathering products which comprise high-Fe-Si-, Si-Mg-Al-, Si-Fe-Al-, Si-Al- and Si-Ti-Al-Fe-Ca-rich alterations. The composition of these late stage alteration products was governed by low-temperature post-magmatic alteration of kaersutite along cleavage planes and fractures.

KEYWORDS: Harrat Ash Sham, Inclusion, Kaersutite megacryst, Sulphide, Iron oxides, Alteration.

1. Introduction

Iron-oxide, sulphide, silicate solid, and melt inclusions have been reported from minerals (e.g. olivine and pyroxene) in igneous rocks of diverse compositions with different cooling histories (e.g. Larocque *et al.,* 2000; Török *et al.,* 2003; Zajacz and Szabó, 2003; Halter *et al.,* 2004a b; Hongfu *et al.,* 2006; Laubier *et al* 2007). Such inclusions in minerals of igneous rocks provide important information on the composition and evolution of magmatic systems (e.g. Andersen and Neumann, 2001; Frezzotti, 2001). However, the composition of solid and melt inclusions in minerals may be controlled by the composition of the host phenocryst and can be affected by processes such as volatile dissociation, oxidation, partial re-equilibration, alteration, and reaction with their host during cooling.

Upper mantle xenoliths and megacrysts of kaersutite as well as clinopyroxene, orthopyroxene and spinel can be found in lava flows and ejecta of the Cenozoic Harrat Ash Sham volcanic field of Jordan and Syria. The kaersutite megacrysts are single crystals and contain multiphase solid inclusions. In this paper, we describe several generations of primary and secondary multiphase solid inclusions in kaersutite megacrysts that occur in Quaternary basaltic rocks from the Harrat Ash Sham volcanic field, Syria. We present textural observations and compositional data of these inclusions and discuss the possible processes which have formed and modified these inclusions.

2. Geologic setting

The Cenozoic Harrat Ash Sham volcanic field is a segment of a widespread volcanic province in the northwestern part of the Arabian Peninsula (Figure 1) which consists of several volcanic fields that are locally called "harrats" (Camp and Roobol, 1992; Nasir, 1994). The Harrat Ash Sham Volcanic Field is noteworthy due to abundant mafic and ultramafic xenoliths, xenocrysts and megacrysts (Nasir, 1992; Nasir *et al.,* 1992; Nasir, 1995; Nasir and Safarjalani, 2000; Al-Mishwat and Nasir, 2003). The emplacement of the Harrat Ash Sham lava was controlled by rifting related to the opening of the Red Sea. K-Ar age dating indicates that most of the volcanism occurred before 14 $\pm$ 1.6 Ma ago (Ilani *et al.,* 2001) compositionally the lavas are mainly alkali olivine basalts and basanites (Nasir, 1994; Lustrino and Sharkov, 2006; Krienitz *et al*., 2006; Shaw *et al.,* 2007). In southern Syria there were three episodes of volcanism – in the Miocene, Pliocene and Quaternary.

These three episodes are petrographically and geochemically indistinguishable (Mouty *et al*., 1992). However, kaersutite megacrysts and mafic and ultramafic xenoliths of lower crustal and upper mantle origin are most common in the Quaternary lavas and are scarce in the Miocene-Pliocene alkali olivine basalts. The petrography and mineral chemistry of these xenoliths are described in detail by Nasir (1992) and Nasir and Safarjalani (2000). The dominant megacryst phases in the Harrat Ash Sham volcanic field are Al-clinopyroxene, ferroan spinel (pleonaste) and kaersutitic amphibole (Nasir, 1995). Pressure-temperature estimations (e.g. 2 pyroxenes Ca in orthopyroxene thermometers, Ca in olivine barometers) suggest that the megacrysts and mafic-ultramafic xenoliths crystallised at temperatures of 900-1050°C and pressures of 12-15 kbar i.e. in the upper mantle near the crust-mantle boundary (Nasir, 1992; Nasir and Safarjalani, 2000).

3. Methods

The samples in this study were collected from the pyroclastic component of the Quaternary alkali-olivine basalt of the Dhanoon volcano in the Harrat Ash Sham Volcanic Field (Figure1). Three megacrysts (M1, M2, and M3) were selected for this study. These specimens contain abundant round to oval-shaped silicate, sulphide, and oxide inclusions. The inclusions were screened by means of transmitted and reflected light microscopy as well as with back-scattered electron imaging (BSE). Mineral analyses were then carried out on representative inclusions at Universität Stuttgart using a CAMECA SX100 electron microprobe. Operating conditions were: 15 kV accelerating

voltage, 10 to 15 nA beam current, 1 to 5 µ electron beam size, and integration time of 20 seconds on peak and on background per analysed element. The standards applied were: corundum (Al), albite (Na), wollastonite (Ca, Si), MgO (Mg), orthoclase (K), rhodonite (Mn), hematite (Fe), barite (Ba), rutile (Ti), NiO (Ni), Cr_2O_3 (Cr), CoO (Co), sphalerite (Zn) and chalcopyrite (Cu, Fe, S). The raw data were corrected using the PAP procedure. No aqueous fluid inclusions were observed in the investigated samples.

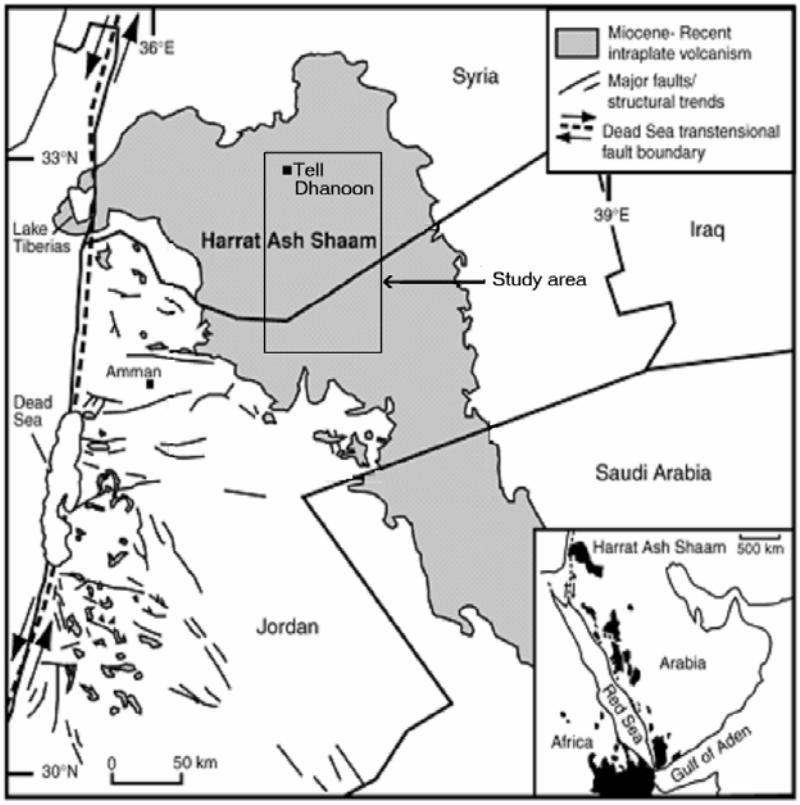

Figure 1. Location map relating to the investigated megacrysts of the Harrat Ash Sham Volcanic Field.

4. Petrography

Amphibole megacrysts occur as black and hypidiomorphic crystals ranging between 5 x 3 x 3 cm and 10 x 5 x 5 cm in size (Figure 2a, b). Most amphibole megacrysts are characterised by numerous inclusions that are distributed irregularly or in patches or are aligned in planes. The inclusions are often bleb-like, rounded, rod-like, elongated or globular (Figures 3a 4a 5a). In case of elongated inclusions, the long axes of rods are oblique to the (110) cleavage planes of the host amphiboles (Figure 4a). In many cases, minute veins containing the same mineral phases as the inclusions connect inclusions (Figures 3c d f and 4a b f). Furthermore, sealed cracks connecting the inclusions are also present. These cracks are often curved and not related to the cleavage planes of the amphibole. The identified inclusion phases comprise various sulphide, oxide and silicate minerals as well as silicate- and/or Fe-rich alteration products. The alteration products are variable in size and shape (Figures 3-5). They occur as birefringent cryptocrystalline aggregates of presumably silicate minerals (e.g. clay, chlorite) and/or iron hydroxides (limonite) filling the spaces between daughter crystals.

Oxide minerals are magnetite, pseudobrookite, and hematite. Pyrrhotite is the major sulphide phase, occurring as rounded or rod like blebs that typically form isolated rounded inclusions. Small amounts of chalcopyrite appear together with pyrrhotite in inclusions of sample M3.

Figure 2a. Photomicrograph showing representative kaersutite megacrysts.

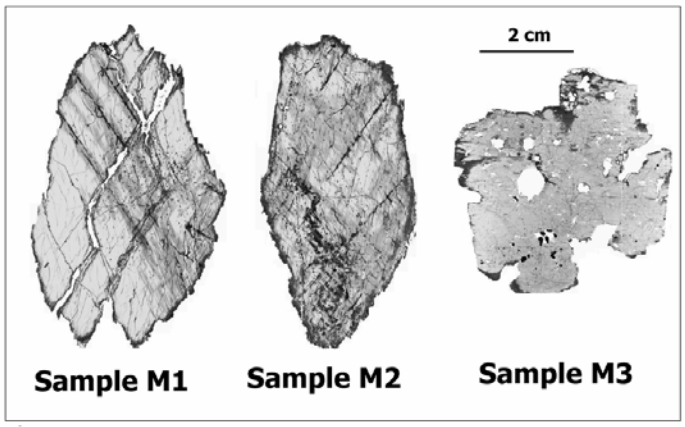

Figure 2b. Scanned image of polished sections showing the distribution of inclusions (black points) within the analyzed samples M1, M2 and M3.

Small crystals of clinopyroxene, orthopyroxene, amphibole, phlogopite, olivine, and plagioclase also occur in the silicate- and/or iron-rich alterations (Figures 3a to f, 4d, e and 5c, d). The kaersutite megacrysts are divided into three types considering the textural arrangement of the inclusions:
(1) **Megacryst Type A** (sample M1; globules a-e in Figure 3): this type contains mostly spherical and rounded inclusions. The size of the inclusions is usually between 100-200 μ, but may occasionally reach up to 300 μ. The megacryst is dominated by magnetite and pyrrhotite inclusions. Interconnecting veins and annealed fracture planes are common (Figure 3a to f). The interfaces of these veins with the host kaersutite are irregular. Very fine-grained aggregates of plagioclase, orthopyroxene, clinopyroxene, phlogopite, amphibole and hematite have been identified

in these veins. Fe-rich- and/or silicate-alterations are widespread in cores of larger magnetite, hematite and pyrrhotite grains.

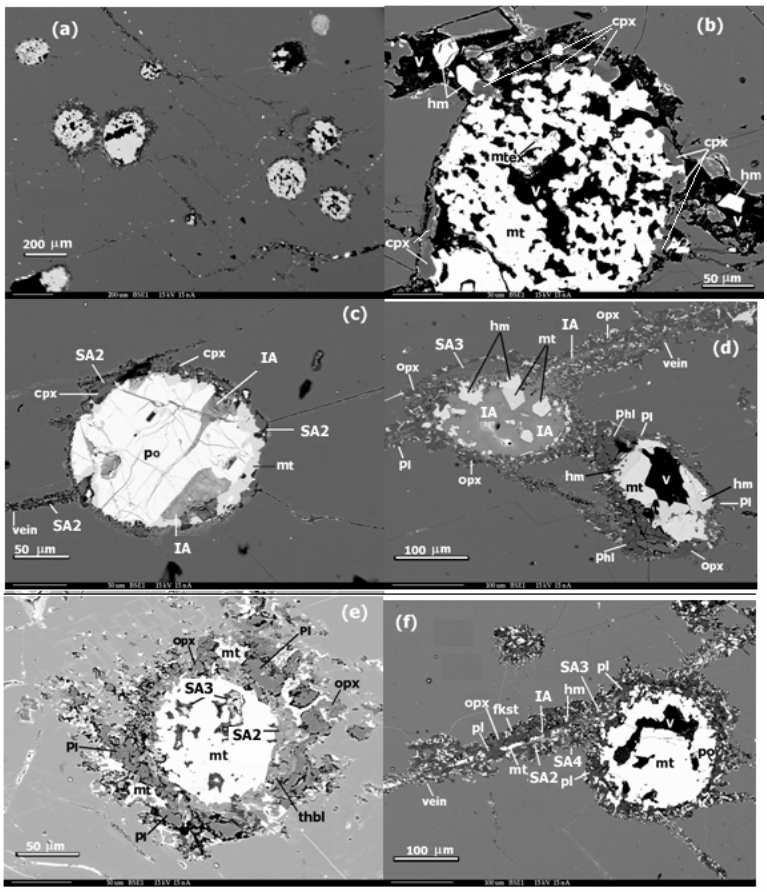

Figure 3. Back scattered electron (BSE) image of Type A inclusions (sampleM1). (a) rounded inclusions. (b) iron-oxide globule within kaersutite (mt, magnetite; mtex, magnetite exsolution, hm, hematite). Black areas at the surface of iron oxides are empty voids (V). Clinopyroxene (cpx) is present as rims surrounding iron oxides. Rounded pyrrhotite (po) inclusions with a rim of magnetite. Clinopyroxene and SA2 and IA crosscut the inclusion (# 1, 2; Table 6-7). (d) Iron-oxide globule surrounded by phlogopite (phl), plagioclase (pl) and orthopyroxene (opx) at the bottom. At the top: inclusion rich in IA (# 3; Table 6) and iron oxide surrounded by plagioclase, orthopyroxene and SA3. (e) Rounded magnetite inclusion bounded by plagioclase orthopyroxene and tschermakitic hornblende (thbl). (f) Magnetite inclusion with voids and bounded by pyrrhotite and plagioclase. A vein cross-cuts the kaersutite and the inclusion. The vein is filled with orthopyroxene, plagioclase, magnetite, hematite, ferrokaersutite (fkst).

(2) **Megacryst Type B** (sample M2; globule a-f in Figure 4) contains inclusions of pyrrhotite, magnetite, hematite, pseudobrookite, clinopyroxene and orthopyroxene. Most of these inclusions have elongated, rod-like outlines ranging in length from 50 to 100 μ, and occur along parallel planes. Interconnecting veins and annealed fracture planes are common (Figure 4a to f). The veins and fractures are filled with fine-grained aggregates (e.g. chlorite and/or clay minerals).

(3) **Megacryst Type C** (sample M3; globules a-f in Figure 5) contains globular inclusions. These inclusions occur as isolated globules within the kaersutite, as well as several globules arranged along cleavage planes of kaersutite. Some globules are associated with open voids (Figure 5a, b).

Most blebs of this type have a droplet shape and range in length from 100 to 1200 µ. Meniscus-shaped boundaries of silicate alteration assemblages are common in open voids (Figure 5b). The inclusion phases comprise pyrrhotite, chalcopyrite, a Ni-Co-S solid solution phase, magnetite, pseudobrookite, hematite, clinopyroxene, olivine and fine-grained alteration products. Along rims and cracks, pyrrhotite is partly replaced by limonite (Figures 4c and 5f)**.** In megacryst M3, empty voids occur associated with hematite inclusions (Figure 5c, d). The shape of hematite and magnetite in these inclusions is rounded and bleb-like. The interior of hematite drops in M3 is often frothy and impregnated by minute holes (Figure 5b, e). Similar frothy hematite globules in olivine were observed by Larocque *et al.* (2000), who interpreted these structures as due to degassing phenomenon.

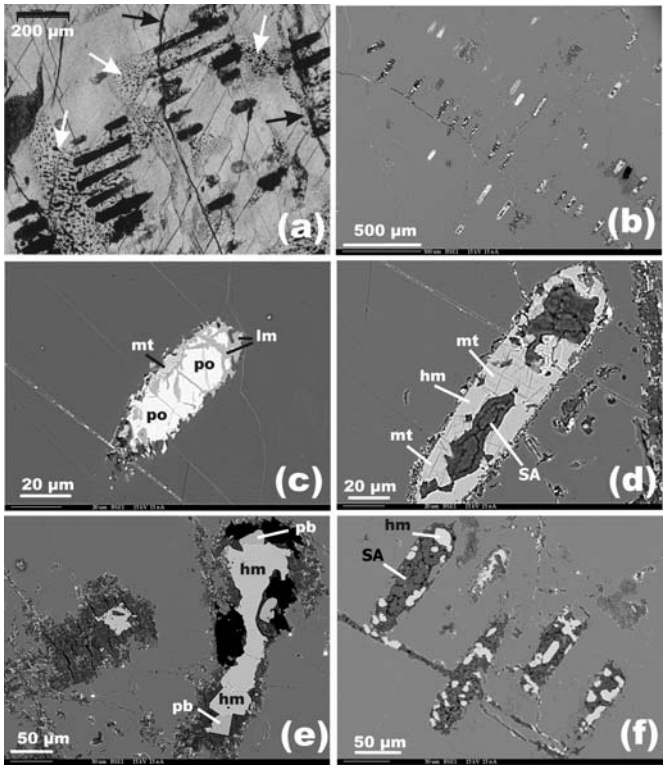

Figure 4. Photomicrographs of inclusions in kaersutite (Type B) sample M2. (a) Oriented inclusions with rod-like outlines in kaersutite. The inclusions appear black due to a high content of oxides. Individual inclusions are interconnected by veinlets containing the same phases (black arrows) or curved crack plans (white arrow). Transmitted light 1 polar. (b) BSE image showing inclusions containing sulphides (white) and silicate alteration (black) in kaersutite. A planar veinlet (upper left to lower right) is interconnecting several inclusions. (c) Pyrrhotite (po) globule partly replaced by limonite (lm). Small amounts of magnetite (mt) are additionally present. (d) Detail of (b) showing a globule composed of slightly exsolved magnetite, hematite (hm) and SA2. (e) Inclusion containing hematite, pseudobrookite (pb) and small amounts of SA (greyish colour). BSE image. (f) Detail of (b) showing inclusions containing SA1 and hematite. Inclusions are interconnected by a veinlet containing the same phases as the inclusions.

5. Chemical compositions of kaersutite and the inclusion phases

5.1 Silicate minerals

The kaersutite host crystals are homogeneous in composition (# 61 to 63, Table 1). No significant chemical zoning has been detected even on the centimeter scale. Mössbauer spectroscopy indicates that all Fe in the kaersutite is Fe^{3+} (Nasir and Al-Rawas, 2006). Thus, they are ferrikaersutite according to the nomenclature of Leake *et al.* (1997). The composition of the kaersutite megacrysts is similar to that of the associated group I and II xenoliths. Amphibole re-crystallisation on small void walls can be easily recognised by a slight change in colour. The bleached kaersutite seams around inclusions are characterised by very low or no Fe^{3+} (# 64, Table 1) according to the calculated formulae. Two additional varieties of amphibole were identified within the inclusions. The first variety which is Al_2O_3-rich and TiO_2-poor occurs in inclusion M1-e (# 65, Table 1). It is a tschermakitic hornblende according to the nomenclature of Leake (1997). The second variety is a ferro-kaersutite, and occurs in inclusion M1-f (# 66, Table 1). This amphibole is Ti- and Fe-rich and Mg-poor.

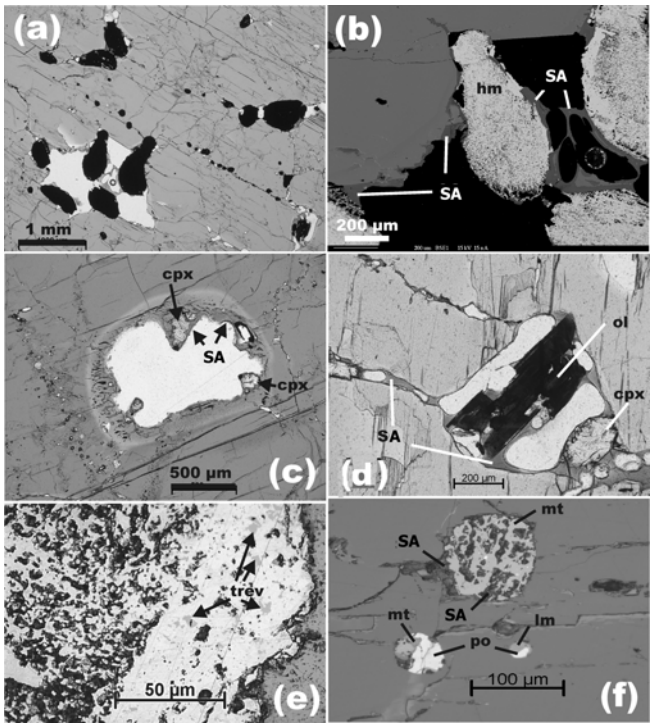

Figure 5. Photomicrographs of inclusions in kaersutite (Type C) sample M3. (a): Black drop-like hematite-rich inclusions in kaersutite. The hematite inclusions are partly linearly arranged along cleavage planes of the amphibole host. Transmitted light, 1 polar. (b) Detail of (a). The BSE image shows frothy hematite droplets (white) and silicate alteration (dark gray) in an open cavity. Meniscuses and rounded voids in the alteration indicate the presence of fluid during the settlement of the melt. (c) Open cavity in kaersutite partly filled by silicate alteration (SA4) and clinopyroxene crystals (cpx). Possible reaction of SA4 with the kaersutite host is indicated by a bleached seam around the inclusion. (d) Open cavity filled by silicate alteration with (oxidised) olivine and clinopyroxene crystals and by voids. Plane polarised transmitted light. (e) Detail of (b) showing frothy hematite with tiny voids (irregular black) and trevorite (trev, intermediate grey reflectance). Plane polarised reflected light. (f) At the top: inclusion of magnetite (mt) with tiny inclusion of a Ni-Co-Fe-S phase

solid solution (white spots) and irregular inclusions of silicate alteration (SA1). Silicate alteration (SA2) is also present at the exterior of the inclusion. Lower half: globules with pyrrhotite (partly replaced by limonite) coexisting with IA. Plane polarised reflected light.

Phlogopite (Mg# (Mg/(Mg + Fe) = 0.94) occurs only in inclusion M1-d (# 67, Table 1). In comparison to phlogopite in associated group I xenoliths, it shows lower contents of Al_2O_3, TiO_2, and Na_2O and higher MgO content.

Olivine up to 0.8 mm occurs in sample M3. This mineral is reddish in colour as if oxidized to fine-grained iddingsite. However, microprobe analyses still yield compositions close to olivine (# 68 and # 69 in Table 6). Variations in Fe and Mg content suggest a zoning of the former olivine. The chemistry of olivine is relatively similar to olivine in host basalt and associated group II xenoliths (Table 1).

Table 1. Representative electron microprobe analyses of amphibole, phlogopite and olivine.

Megacryst	M1	M2	M3	M3	M1		I	II	M1	II	M3		I	II	Bas.
Globule	host			c	e	f			d		d				
Analysis #	61	62	63	64	65	66			67		68	69			
Mineral	Krs			blkrs	thbl	fkrs	krs		phl		ol				
											Core	rim			
SiO_2	39.61	40.34	40.67	38.97	44.56	37.69	39.52	39.63	41.33	37.1	41.62	40.85	40.66	39.13	39.8
TiO_2	5.76	5.44	5.31	6.97	0.17	5.71	4.48	5.27	3.8	5.73	0.07	0.05	0	0	0
Al_2O_3	14.9	14.6	14.63	14.99	19.75	16.57	14.94	14.18	11.8	16.65	0.06	0.09	0	0	0
Cr_2O_3	0	0.02	0	0.01	0	0	0	0	0	0	0	0.02	0	0	0
Fe_2O_3	11.41	11.53	11.48	0	2.83	0	0	0	0	0	0	0	0	0	0
FeO	0	0	0	8.67	8.8	23.55	12.48	13.12	3.08	6.9	11.95	19.25	9.46	17.8	16.32
Ni	0.03	0	0	0.04	0.11	-	-	-	0.28	0	0.02	0.04	0.38	0.47	-
MnO	0.13	0.05	0.1	0.11	0.07	1.41	0.15	0.14	0.01	0	0.24	0.1	0.28	0.21	0.22
MgO	13.18	13.4	13.3	13.55	13.61	1.33	12.14	12.87	24.8	17.55	46.73	41.3	48.99	41.78	43.14
CaO	10.25	10.32	10.53	11.69	8.57	11.3	11.62	10.57	0.03	0.05	0.2	0.26	0.04	0.04	0
Na2O	3.14	2.38	2.71	2.44	0.77	0.18	1.65	1.45	0.18	1.35	0	0	0	0	0
K2O	1.51	2.04	1.71	1.46	0.2	0.28	0.69	0.95	9.86	9.71	0	0	0	0	0
BaO	0	0.18	0.13	0.2	0	0	0	0	0	-	0	0	0	0	0
Total	99.92	100.3	100.57	100.91	99.39	98.13	97.69	98.21	95.17	95.7	100.64	101.91	99.83	99.43	99.7
Mg#	0.7	0.7	0.7	0.73	0.69	0.09	0.63	0.63	0.94	0.85	0.86	0.79	0.9	0.8	0.81
	Cations on the basis of														
	23 (O)								22 (O)		4 (O)				
Si	5.628	5.697	5.725	5.675	6.206	5.833	5.852	5.847	5.842	5.445	1.025	1.028	0.998	1.002	1.008
Ti	0.616	0.578	0.562	0.741	0.018	0.665	0.500	0.585	0.404	0.369	0.001	0.001	0.000	0.000	0.000
Al	2.495	2.430	2.427	2.573	3.241	3.023	2.607	2.466	1.966	2.805	0.002	0.003	0.000	0.000	0.000
Cr	0.000	0.002	0.000	0.000	0.000	0.000	0.000	0.000	0.000	0.000	0.000	0.000	0.000	0.000	0.000
Fe^{3+}	1.220	1.225	1.216	0.000	0.296	0.000	0.000	0.000	0.000	0.000	0.000	0.000	0.000	0.000	0.000
Fe^{2+}	0.000	0.000	0.000	1.056	1.024	3.048	1.545	1.620	0.364	0.789	0.246	0.405	0.195	0.381	0.346
Mn	0.016	0.006	0.012	0.014	0.008	0.185	0.019	0.017	0.001	0.000	0.005	0.002	0.006	0.005	0.005
Mg	2.792	2.821	2.791	2.941	2.823	0.307	2.680	2.831	5.226	4.442	1.716	1.552	1.792	1.591	1.698
Ni	0.001	0.000	0.000	0.000	0.001	0.012	0.000	0.000	0.050	0.000	0.001	0.001	0.012	0.015	0.000
Ca	1.561	1.562	1.588	1.824	1.278	1.874	1.844	1.672	0.005	0.000	0.005	0.007	0.001	0.001	0.006
Na	0.865	0.652	0.740	0.690	0.208	0.054	0.474	0.415	0.049	0.097	0.000	0.000	0.000	0.000	0.000
K	0.274	0.367	0.307	0.271	0.036	0.055	0.130	0.179	1.778	1.770	0.000	0.000	0.000	0.000	0.000
Ba	0.000	0.044	0.032	0.011	0.000	0.000	0.000	0.000	0.000	0.000	0.000	0.000	0.0000.	0.000	0.000
Total	15.468	15.384	15.399	15.796	15.056	15.651	15.632	15.684	13.646	15.717	3.001	3.035	3.004	2.995	2.992

Fe_2O_3/FeO ratio determined by Mössbauer (# 61,62,63) or according to Holland & Blundy (1994) (# 64,65,66).
krs: subcalcic kaersutite, thbl: tschermacitic hornblende, fkrs: ferro-kaersutite, phl: phlogopite, ol: olivine.
I, II, Bas: Representative mineral analyses from Group I and II xenoliths and basalts from the same area (Nasir, 1992, 1995).

Clinopyroxene is diopsidic in composition (Wo45-46En33-42 Fs10-19) in inclusions M1-b and M1-c (Figure 5 b-c # 53-54, Table 2) whereas that from inclusions M2-e and M3-c (Figures 4e and 4c, # 55-56) is augitic (Wo36-42En 46-53Fs9-10) according to the pyroxene nomenclature of Morimoto *et al.* (1988). The Mg# of clinopyroxenes from megacrysts M1 (# 53-54) varies between 0.68 and 0.71, which is lower than the Mg# of pyroxenes from host basalts and associated xenoliths (0.8-0.92). However, clinopyroxenes from inclusions M2 and M3 are similar in their Mg# (0.82-0.85) to Mg# (0.8-0.83) of host basalt and group II xenoliths from the same area (Nasir, 1992).

Orthopyroxenes were detected only in inclusions M1 (d, e, f) and M2-d (# 57 to 60, Table 2)**.** The Mg# of this mineral is variable (0.81-0.92). Orthopyroxene from inclusion M2-d (# 60) is poor in Al_2O_3 (3.91 wt.%) compared with those from M1(# 57 to 59, Table 2). The orthopyroxenes in the inclusions of megacryst M1 have Mg# of 0.81 to 0.85, which is similar to the Mg# of orthopyroxenes from associated megacryst and group II xenoliths from the same area, while orthopyroxene from megacryst M2 (#60, Table 2) is similar in Mg# (0.92) to clinopyroxenes from associated group I xenoliths.

Plagioclase occurs only in inclusions d, e, and f (Figure 3d) of the megacryst M1 (# 70 to 72, Table 3). The plagioclase compositions (An_{73-75}) are similar in all inclusions. The An-content of this plagioclase is higher than the An-content in the host basalt (An_{40-50}).

5.2 Iron oxide minerals

Magnetite occurs in four compositional varieties: type (1) magnetite coexists mostly with pyrrhotite (samples M1 and M2) and shows exsolution lamellae of another type of magnetite (type 2). Type1 magnetite is poor in Al_2O_3 and MgO (#20, 27, Table 4) whereas the lamellae (type 2) show higher Al and Mg contents (# 21 and 28, Table 4). Type 3 magnetite, without exsolution lamellae, coexists mostly with hematite, sulphide, IA and/or SA (# 25, 29, 33, Table 4). The chemical composition of this type of magnetite is variable. Type 4 magnetite coexists with hematite. It is enriched in NiO and CoO, and may even reach trevorite composition (# 30, Table 4). Primary magnetite is altered to hematite along individual cracks, particularly near open cracks or cavities (Figures 3d, f, 4b, f). A representative analysis of a pseudobrookite occurring in sample M2 and M3 is given in Table 4 (# 34-35). According to the calculated formula, it contains no Fe^{2+} but a significant karooite ($MgTi_2O_5$) and lesser tielite (Al_2TiO_5) component.

Three types of hematite have been identified. Type 1 hematite occurs in iron alteration (IA) and/or silica alteration (SA) (# 36, 42, Table 4) and shows only minor amounts of the ilmenite component in comparison to Type 2 hematite, which is associated with magnetite (# 37, 41; Table 4). Type 3 hematite occurs in blebs of SA inclusions and is close to the end-member composition (# 45, Table 4).

5.3 Sulphide minerals

Pyrrhotite is the principal sulphide phase in the inclusions. In the structural formula normalised to one sulphur, the cation total ranges between 0.88 and 0.93 (# 46 to 50, Table 5). In samples M1 and M2, pyrrhotite mostly occurs as single-phase inclusions (54) or Ni-Co-Fe-S phase solid solution (33 wt.% NiO and 18 wt.% CoO; # 52, Table 5) occurs as tiny (up to 5 μm in size) inclusions in magnetite. Chalcopyrite associated with Ni poor pyrrhotite was observed only in M3 (# 51, Table 5). The sulphide compositions resemble those reported from sulphides in clinopyroxene megacrysts and sulphide inclusions of Type-I xenoliths from several localities globally (Figure 6) (Zajacz and Szabó, 2003).

5.4 Alteration phases

Tables 6 and 7 summarize the electron microprobe data for the different alterations phases in the inclusions. Two main types of alteration products are found: iron-rich alteration (IA) and silicate alteration (SA). Analyses of SA and IA show low and variable anhydrous totals of 74 to 92 wt.% and 85 to 97 wt.% respectively. Similar observations were made by Stimac and Hicmott (1996) and Larocque *et al*. (2000) on comparable iron-rich inclusions. These authors attributed such low totals to the frothy nature of the inclusions.

Another and more probable reason for obtaining low totals in the microprobe analyses could be the volatile content in the alteration products of the inclusion (e.g. Churikova *et al.* 2007). The silicate minerals (e.g. hornblende, pyroxene, phlogopite and plagioclase) are altered to fine grained products ("clay minerals and/or chlorite"), particularly in sample M2.

5.4.1 Iron-rich alteration (IA)

IA is associated with magnetite, hematite, or pyrrhotite inclusions. It shows high Fe_2O_{3total} (80-89 wt.%), low MgO (0.2- 3.3 wt %), and variable SiO_2 (12-19 wt%), CaO (0.16-2.4 wt%), TiO_2 (0.02-0.2 wt%) contents, and contains appreciable NiO (0.1-0.9 wt%). Contents of alkali oxides (0.02-0.1 wt.%) are negligible (Table 6). Hurai *et al*. (1998) and Larocque *et al.* (2000) observed similar compositional ranges for high iron glass inclusions in olivine megacrysts (Table 6). However, the IA compositions in Table 6 do not look like they were originally silicate melts or glasses, but are most probably iron hydroxides.

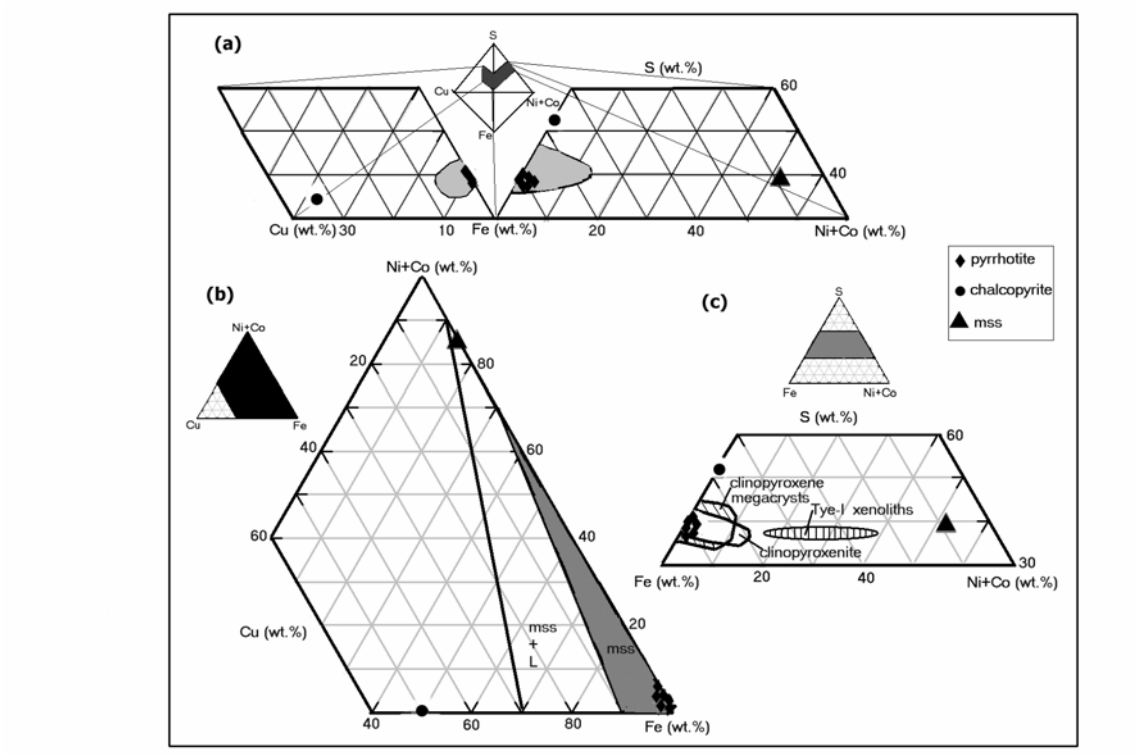

Figure 6. Bulk sulphide compositions plotted in (a) Cu-Fe-(Ni+Co) system. (b) Fe-(Ni+Co)-Cu system. The stability field of monosulphide solid solution (mss) at 1100°C based on experimental studies by Kullerud *et al.* (1969). (c) Bulk sulphide compositions compared to compositions of sulphides in Type I xenoliths and clinopyroxene megacrysts (Zajacz and Szabó, 2003).

5.4.2 Silicate alteration (SA)

The anhydrous total of SA always shows a clear deficit compared to 100% total, which is attributed to alteration of silicate minerals to hydrous phases (e.g. chlorite and/or clay minerals). During this alteration, the original composition was modified. The extent of this compositional modification is difficult to assess. Four groups of SA compositions have been identified (Table 7). The first (SA1) is associated with hematite and contains 41 to

48 wt.% SiO_2 with some MgO and Al_2O_3 as sole constituents of importance. CaO is only present in subordinate amounts in SA1 (# 6 ,7; Table 7). In contrast, SA occurring with magnetite (SA2) contains 36 to 44 wt.% SiO_2, higher Al_2O_3 and lower MgO content. In addition, 3.7 to 7.8 wt. % of Fe_2O_{3total} are present in SA2 (# 8 to 11, Table 7). Other oxide components are subordinate. Both alteration products (SA1 and SA2) are comparable in composition to clay minerals (e.g. saponite and/or vermiculite) and thus could be mainly composed of such phases. SA3 was found mainly in M1 inclusions. It is represented by a Fe-Al-rich alteration product with a composition similar to Fe-rich chlorite and/or chloritic alteration in terms of its Fe_2O_3- (29-42 wt.%), Al_2O_3- (19-22 wt. %), and SiO_2-content (21-26 wt.%). MgO, CaO, TiO_2, MnO, and alkalis are minor and range between 0.01 and 2.8 wt. % each (# 12 to 14, Table 7). Brownish-coloured silicate alteration (SA4) is present in open cavities and at the rims of inclusions of sample M3. Under reflected light, this alteration shows abundant reddish internal reflections pointing to the presence of Fe^{3+}-rich minerals. SA4 is similar in composition to the kaersutite host. Remarkable is the relatively high content of TiO_2 in SA4, ranging between 5.4 and 6.2 wt.% (# 15 to 19, Table 7). The main chemical variability of SA4 concerns the Fe_2O_3 content ranging between 13.9 and 20.0 wt. %.

6. Discussion

Kaersutite crystallizes from mafic and ultramafic melts at medium pressures, somewhat below 10 kbar, high temperatures (>950^oC) and moderate oxygen fugacity (Oba, 1997; Ernst and Liu, 1998). Hops *et al*., (1992) proposed a model of megacryst formation from localized melt segregations within the lithosphere. Boettcher and O'Neil (1980) and Ionov *et al.,* (1997) presented evidence that metasomatism of upper mantle lherzolite by aqueous fluids rich in TiO_2, K_2O and FeO is responsible for the production of kaersutite.

Conformably, studies of mantle xenoliths from Jordan and Syria show that the formation of the Harrat Ash Sham Volcanic Field over the last 40 million years was accompanied by extensive mantle metasomatism (Altherr *et al* 1990; Nasir ,1992; Nasir and Safarjalani, 2000). Henjes-Kunst *et al*. (1990) showed that the lithospheric mantle beneath the Arabian Peninsula formed from the same source as the overlying juvenile crust – at about 700 Ma. Henjes-Kunst *et al*. (1990) identified two metasomatic events in the sub-continental lithosphere, the second of which they related to mantle processes connected to the formation of the Red Sea. The megacryst suite of the Harrat Ash Sham Volcanic Field comprises large unzoned single grains of clinopyroxene, orthopyroxene, spinel and kaersutite. These megacrysts have a limited range of compositions (Nasir, 1995). Major and trace-element partitioning in the kaersutite megacrysts indicates that they equilibrated with their host magmas (Nasir, 1995). The monomineralic nature of the megacrysts suite, their large size and homogeneity, and their uniform composition suggest crystallization from a hydrous melt. The megacryst assemblages are interpreted as high-pressure phenocrysts associated with the formation and partial crystallization of a hydrous basanitoid melt at depth. The abundant presence of kaersutite and its association with other phases implies the formation of a hydrous melt at a depths estimated to be 40-50 km (Nasir and Safarjalni, 2000). (This hypothesis is very testable by comparing REE and trace element patterns of megacrysts with basanite REE and trace element patterns).

The mineral composition of primary minerals (magnetite, pyrrhotite) of the inclusions in the three kaersutite megacrysts are extremely heterogeneous both in terms of phase compositions and phase proportions. The inclusions lack a visible melt and fluid phase (i.e. H_2O, CO_2). However, the former presence of a fluid phase may be assumed because of the regular presence of one or more deformed cavities (voids) within most inclusions (Figures 3-5)**.** The formation of solid inclusions in these kaersutites as manifested by the typical round to oval shapes could be due to trapping of melt residue from the basanitoid magma which may have penetrated the fractured kaersutite during crystallisation. The spherical shape of some magnetite inclusions and some negative crystal-shaped oriented inclusions suggests their enclosure during the growth of the host amphibole. Formation of some inclusions contemporaneous with the growth of kaersutite is an attractive explanation because of the parallel arrangement of the long axes of inclusions (Figure 4) which may represent former kaersutite growth planes as proposed by Andersen *et al.* (1987) and Zajacz and Szabó (2003). However, from the textural descriptions and the BSE images (Figures 3 to 5) it appears that most inclusions are secondary in origin, i.e. trapped along cracks in kaersutite after it had already crystallised. (Could rod-like inclusions reflect exsolution phenomenon?).

Some inclusions are interconnected by veins containing the same assemblages as the inclusions. These veins are interpreted as former cracks that partly exploited kaersutite cleavage planes. Sub-parallel fractures combined with breaks along the cleavage divide the crystals into small fragments. In sample M3 a suite of inclusions can be observed ranging from ovoid droplets in open voids to rounded inclusions completely enclosed by amphibole (Figure 5a). This observation suggests that the trapping of some of the inclusions occurred in open cracks. An additional argument for a secondary origin of most inclusion is that the host kaersutite was not in chemical equilibrium with the trapped melt. In most globules, the host amphibole-inclusion interface is not smooth but irregular and shows an intimate interlocking of silicates with kaersutite (Figures 3d, e, f, and 4c, e, c). The irregular interfaces of the inclusions and veins with the host kaersutite which show resorption and melting of the host, might be connected with the infiltration and thermal effect of the basalt.

Table 2. Representative electron microprobe analyses of pyroxenes.

Megacryst	M1		M2	M3	CPX	I	II	Bas	M1			M2	OPX	I	II
Globule	b	c	e	c					d	e	f	d			
Analysis #	53	54	55	56					57	58	59	60			
Mineral	Clinopyroxene								Orthopyroxene						
SiO_2	50.57	52.33	50.73	49.58	50.50	53.30	49.10	49.90	52.35	53.15	51.39	55.44	53.45	56.90	54.30
TiO_2	0.30	0.26	1.24	1.73	1.65	0.22	1.08	1.63	0.27	0.16	0.15	0.43	0.22	0.00	0.20
Al_2O_3	2.62	3.32	4.92	6.64	6.35	3.30	9.04	4.88	6.46	5.35	6.82	3.91	4.75	2.80	5.50
Cr_2O_3	0.01	0.00	0.01	0.12	0.00	0.00	0.00	0.28	0.00	0.04	0.03	0.00	0.00	0.00	0.00
Fe_2O_3	5.72	0.00	2.10	2.52	0.31	0.00	2.15	1.10	0.00	1.71	3.98	0.38	0.68	0.00	0.00
FeO	4.80	10.43	4.10	3.87	5.27	2.20	3.60	5.85	11.34	8.11	6.73	4.07	9.74	5.45	9.80
MnO	0.11	0.18	0.08	0.12	0.20	0.15	0.05	0.01	0.20	0.16	0.20	0.21	0.10	0.10	0.13
MgO	12.67	12.71	18.68	15.53	14.95	16.30	14.30	14.35	27.82	30.02	29.72	33.86	29.55	34.45	29.80
NiO	0.27	0.02	0.00	0.00	0.00	0.00	0.00	0.00	0.01	0.24	0.21	0.26	0.00	0.00	0.00
CaO	21.41	19.22	17.71	19.61	18.95	22.10	20.04	21.87	0.97	1.10	0.75	0.75	0.85	0.50	0.85
Na_2O	1.14	0.81	0.28	0.88	1.20	0.80	1.04	0.37	0.02	0.02	0.06	0.09	0.10	0.00	0.00
K2O	0.02	0.12	0.08	0.00	0.00	0.00	0.00	0.00	0.10	0.04	0.02	0.08	0.00	0.00	0.00
Total	99.64	99.40	99.93	100.60	99.38	98.37	100.40	100.20	99.54	100.08	100.07	99.47	99.44	100.20	100.60
Mg#	0.71	0.68	0.85	0.82	0.83	0.92	0.82	0.80	0.81	0.85	0.84	0.92	0.84	0.92	0.84
Formulae on the basis of 4 cations (6 oxygen)															
Si	1.896	1.846	1.844	1.805	1.853	1.958	1.784	1.843	1.861	1.863	1.805	1.910	1.890	1.950	1.880
Ti	0.008	0.014	0.034	0.047	0.046	0.006	0.030	0.045	0.007	0.004	0.004	0.011	0.006	0.000	0.005
Al	0.116	0.344	0.211	0.285	0.275	0.143	0.387	0.212	0.271	0.221	0.282	0.159	0.198	0.113	0.227
Cr	0.000	0.000	0.000	0.003	0.000	0.000	0.000	0.008	0.000	0.001	0.001	0.000	0.000	0.000	0.000
Fe^{3+}	0.162	0.041	0.056	0.069	0.009	0.000	0.059	0.031	0.000	0.045	0.105	0.010	0.018	0.000	0.000
Fe^{2+}	0.150	0.289	0.124	0.118	0.162	0.068	0.110	0.179	0.337	0.238	0.198	0.117	0.288	0.156	0.286
Ni	0.013	0.000	0.000	0.000	0.000	0.000	0.000	0.000	0.000	0.011	0.000	0.011	0.000	0.000	0.000
Mn	0.003	0.004	0.003	0.004	0.006	0.005	0.002	0.000	0.006	0.005	0.006	0.006	0.003	0.003	0.004
Mg	0.708	0.574	1.013	0.843	0.818	0.893	0.775	0.790	1.474	1.569	1.556	1.739	1.558	1.760	1.553
Ca	0.860	0.784	0.690	0.765	0.746	0.870	0.780	0.865	0.037	0.041	0.029	0.028	0.032	0.018	0.033
Na	0.082	0.100	0.020	0.620	0.085	0.057	0.074	0.025	0.001	0.000	0.004	0.006	0.007	0.000	0.000
K	0.000	0.002	0.004	0.000	0.000	0.000	0.000	0.000	0.005	0.002	0.002	0.004	0.000	0.000	0.000
Total	4.000	4.000	4.000	4.000	4.000	4.000	4.000	4.000	4.000	4.000	4.000	4.000	4.000	4.000	4.000
Woll	45.7	46.4	36.6	42.5	42.1	47.5	45.2	47.0	2.0	2.2	1.5	1.3	1.7	1.3	1.7
En	37.6	33.9	53.7	46.9	47.4	48.8	44.7	42.0	81.0	82.7	82.2	92.0	82.2	90.0	83.0
Fs	16.7	19.7	9.7	10.6	10.5	3.7	11.1	11.0	17.0	15.2	16.3	6.7	16.1	8.7	15.3

Fe_2O_3/FeO ratio determined from stoichiometry
CPX, OPX: Representative clinopyroxene and orthopyroxene megacrysts, respectively from the same area (Nasir, 1995). Bas.: Representative clinopyroxene from associated basalt (Nasir, 1995), I, II: Representative clinopyroxene and orthopyroxene from Group I and II xenoliths from the same area (Nasir, 1992).

Table 3. Representative electron microprobe analyses of Plagioclase.

Megacryst	M1		
Globule	d	e	f
Analysis #	70	71	72
SiO_2	48.19	49.3	49.86
TiO_2	0.14	0.04	0.11
Al_2O_3	32.11	31.74	31.11
Fe_2O_3	1.05	0.93	1.24
MgO	0.28	0.06	0.14
CaO	14.96	14.88	14.9
Na_2O	2.5	2.63	2.85
K_2O	0.41	0.52	0.35
Total	99.64	100.1	100.56
Cations on the basis of 8 oxygen			
Si	2.220	2.257	2.274
Ti	0.005	0.001	0.004
Al	1.743	1.713	1.672
Fe^{3+}	0.037	0.032	0.043
Mg	0.019	0.004	0.010
Ca	0.738	0.730	0.728
Na	0.223	0.233	0.252
K	0.024	0.030	0.020
Total	5.009	5.000	5.003
An	0.75	0.74	0.73
Ab	0.23	0.23	0.25
Or	0.02	0.03	0.02

The texture of the rods and globules in the kaersutite resembles the anorthosite-calcite rods within kaersutite megacrysts described by Wallace (1977) and the sub-parallel tubular voids in labradorite phenocrysts described by Gutmann (1974). Wallace suggested that the rods are large elongate fluid inclusions that resulted from the growth of gaseous "bubbles" on the crystal contemporaneously with the crystal growth. He interpreted the anorthoclase and calcite as secondary filling of rods in the kaersutite. Gutmann (1974) suggested that the tubular voids in labradorite resulted from nucleation of a gas phase. The pyroclastic breccia of Harrat As Sham volcanoes, including Dhanoon volcano, were the results of multiphase volatile-rich explosive eruptions (Nasir and Safarjalani, 2000). During eruption the kaersutite megacryst was broken up and veins and fractures were filled by melts from which silicate minerals crystallized. The kaersutite host crystals are homogeneous in composition, which implies that there were no reactions between kaersutite and the invading melt. Most analyses of kaersutite, pyroxene, and olivine show them to be relatively similar in their chemistry to those in host basalt and associated group II xenoliths, which supports the argument that most of the silicate minerals were formed through crystallisation from invading melt. However, a few analyses of silicate minerals (e.g., hornblende # 65-66, Table 1, phlogopite # 67, Table 1 and clinopyroxene #53-54, Table 2) show them to have compositions remarkably different from the minerals of the host basalt and upper mantle xenoliths. Their occurrence may reflect open system differentiation, recrystallization and/or localized decompression melting inside the inclusions which could generate mineral paragenesis different from that

of the host basalt.

Table 4. Representative electron microprobe analyses of iron-oxides.

Megacryst	M1	M2			M2			M3		M2	M3	M1	M2	M3	
Globule	b	b	f	d	d	d	e	f	e	d	b	d	d	f	e
Analysis #	20	21	25	27	28	29	30	33	34	35	36	37	41	42	45
Oxide	mt	mtex.	mt	mt	mtex	mt	mt	mt	pb	pb	hm	hm	hm	hm	hm
Type	1	2	3	1	2	3	4	3			I	II	II	I	III
TiO_2	0.71	0.24	0.16	0.27	0.59	1.04	0.00	0.03	41.84	41.94	8.57	23.48	13.56	6.00	0.25
Al_2O_3	0.40	4.49	0.12	1.15	18.63	3.71	0.04	0.11	1.36	3.96	1.32	0.58	0.75	0.98	0.10
Cr_2O_3	0.02	0.11	0.01	0.01	0.00	0.00	0.00	0.00	0.02	0.08	0.06	0.01	0.01	0.12	0.01
Fe_2O_3	67.25	72.82	71.55	69.07	52.04	66.39	68.31	69.28	52.09	46.79	83.25	57.81	74.54	89.02	99.93
FeO	31.04	1.08	21.58	22.24	17.55	19.43	4.43	30.03	0.00	0.00	0.00	15.60	7.86	0.00	0.14
MnO	0.12	0.79	0.04	0.22	0.20	0.39	0.81	0.02	0.01	0.19	0.31	0.03	0.04	0.66	0.01
MgO	0.23	16.03	6.25	4.29	10.08	7.49	0.94	0.25	4.19	5.16	3.93	2.63	2.31	3.05	0.03
NiO	0.16	6.44	0.05	2.00	1.54	1.00	17.67	0.67	0.00	0.00	0.69	0.51	0.11	0.06	0.00
CoO	0.00	0.00	0.00	0.36	0.42	0.22	7.15	0.15	0.03	0.00	0.00	0.00	0.07	0.00	0.02
CaO	0.07	0.00	0.03	0.00	0.00	0.00	0.00	0.00	0.00	0.00	0.00	0.00	0.00	0.00	0.00
Total	99.99	100.06	99.89	99.60	101.05	99.68	99.34	100.55	99.54	98.95	98.13	100.65	99.25	99.89	100.50
						Formulae on the basis of									
	3 cations									2 cations					
Ti	0.020	0.006	0.003	0.007	0.014	0.028	0.000	0.007	1.201	1.193	0.166	0.444	0.264	0.116	0.001
Al	0.018	0.174	0.005	0.050	0.708	0.156	0.002	0.049	0.061	0.176	0.040	0.017	0.023	0.030	0.000
Cr	0.001	0.003	0.000	0.000	0.000	0.000	0.000	0.000	0.000	0.002	0.001	0.000	0.000	0.002	0.000
Fe^{3+}	1.939	1.807	1.977	1.934	1.263	1.787	1.998	1.994	1.498	1.332	1.618	1.096	1.450	1.720	1.996
Fe^{2+}	0.992	0.030	0.662	0.692	0.473	0.581	0.144	0.961	0.647	0.000	0.000	0.328	0.170	0.000	0.000
Mn	0.004	0.022	0.001	0.007	0.006	0.012	0.027	0.001	0.000	0.006	0.007	0.001	0.001	0.014	0.002
Mg	0.014	0.689	0.342	0.238	0.485	0.399	0.054	0.014	0.238	0.291	0.151	0.099	0.089	0.117	0.000
Ni	0.008	0.267	0.002	0.060	0.040	0.029	0.552	0.021	0.000	0.000	0.022	0.016	0.002	0.001	0.000
Co	0.000	0.000	0.000	0.011	0.011	0.006	0.223	0.005	0.000	0.000	0.000	0.000	0.001	0.000	0.001
Ca	0.003	0.000	0.001	0.000	0.000	0.000	0.000	0.000	0.000	0.000	0.000	0.000	0.000	0.000	0.000
Total	3.000	3.000	3.000	3.000	3.000	3.000	3.000	3.000	3.000	3.000	2.000	2.000	2.000	2.000	2.000

mt: magnetite, mtex.: magnetite exsolution lamellae, pb: pseudobrookite, hm: hematite 1 to 4: type of magnetite, I-III: type of hematite. Fe_2O_3/FeO ratio determined from stoichiometry.

SA and IA are extremely heterogeneous both in terms of composition (Tables 6-7) and included phase proportions. The IA are dominated by hematite and limonite, while the SA are dominated by chloritic phase and some other clay minerals (SA1-3), and/or kaersutite alteration (SA4). Silicate alteration may represent vein-fillings crystallized from an invading melt and/or they may have formed by alteration of silicate minerals with the last, H_2O-rich melt fraction. This suggests variable growth histories and/or more probably low temperature late-magmatic or subsolidus alterations of kaersutite, iron oxides and infilling silicates along the cleavage planes (Figure 5), fractures (Figure 6a, b, and d) and around sulphide inclusions (Figure 4). Magnetite is altered to hematite along cracks and cavities (Figures 23, f, 5b, f). This well known martitic alteration of primary magnetite was obviously a post-trapping process. The presence of Ni-rich magnetite (trevorite) inclusions in hematite may reflect such an oxidation reaction: magnetite (ss) + O_2 => hematite + trevorite.

Table 5. Representative electron microprobe analyses of sulfides.

Megacryst	M1		M2	M3			
Globule	c	f	c	f			
Analysis #	46	47	48	49	50	51	52
Mineral	po					cp	mss
Fe	60.26	60.26	59.55	59.72	57.46	31.83	8.64
Ni	2.23	1.44	0.83	0.91	2.90	0.21	33.29
Co	0.00	0.00	0.27	0.18	0.42	0.01	17.90
Cu	0.00	0.00	0.01	0.00	0.05	32.59	0.07
Zn	0.00	0.00	0.05	0.00	0.00	0.04	0.00
S	38.34	38.45	39.48	39.15	39.10	35.03	39.62
Total	100.83	100.15	100.18	99.95	99.93	99.71	99.52
Fe	0.902	0.900	0.866	0.876	0.844	0.522	0.125
Ni	0.032	0.020	0.011	0.013	0.040	0.003	0.459
Co	0.000	0.000	0.004	0.002	0.006	0.000	0.246
Cu	0.000	0.000	0.000	0.000	0.001	0.470	0.001
Zn	0.000	0.000	0.001	0.000	0.000	0.000	0.000
Total	0.934	0.920	0.882	0.891	0.891	0.995	0.831
S	1.000	1.000	1.000	1.000	1.000	1.000	1.000

po: pyrrhotite, cp: chalcopyrite, mss: Ni-Co-S monosulfide solid solution**.**

Table 6. Representative electron microprobe analyses of iron-rich alteration (IA) in inclusions from kaersutite megacryst in comparison to high-iron glass in igneous xenoliths from the Carpathians (Hurai *et al*., 1998) and in volcanic rocks from the Philippines, Mexico, USA and Japan (Larocque *et al*., 2000).

Megacryst	M1				M3		
Globule*	c	c	d	e	f	C	PJ
Analysis #	1	2	3	4	5		
SiO_2	12.45	19.50	14.35	12.58	15.98	10.83	2.08
TiO_2	0.07	0.19	0.09	0.02	0.07	0.15	0.18
Al_2O_3	1.86	1.28	0.05	0.17	0.00	0.51	0.81
Fe_2O_3	79.87	87.71	81.75	82.85	89.03	78.69	80.14
MnO	0.10	0.11	0.04	0.00	0.01	1.11	-
MgO	3.34	3.17	0.18	0.18	0.15	0.36	-
NiO	0.41	0.88	0.46	0.54	0.14	0.00	0.88
CaO	0.16	0.47	1.96	1.89	2.43	0.58	0.00
Na2O	0.00	0.08	0.01	0.05	0.00	0.03	0.00
K2O	0.02	0.23	0.05	0.04	0.00	0.06	0.00
CuO	0.00	0.00	0.00	0.00	2.46	0.00	0.00
S	0.10	0.06	0.18	0.41	0.00	0.84	
Total	86.68	94.56	88.90	90.28	96.55	85.91	88.50

Globule*: (a to f) refers to Figures 2 to 4.
C: average of 6 samples from Hurai *et al*. (1998). PJ: average of 26 samples from Larocque *et al*. (2000).

After formation of the host kaersutite, circulating fluids may have interacted with pre-existing inclusions. In this way, the original chemical signature of the inclusions would be lost. Alteration processes such as zeolitization of the volcanic tuff (e.g., Dwairi, 1998; Ibrahim and Hall 2004) and post-magmatic deutric iddingsitization of olivine in the host basalt and associated xenoliths is a widespread phenomenan in the Harrat Ash Sham volcanic field (e.g., Nasir and Mahmood, 1991).

TiO_2-rich silicate alteration (SA4) is present at inclusion rims of sample M3. The composition of this alteration is similar to that of the kaersutite host (# 15 to 19, Table 7). The composition of the participating Ti-rich silicate alteration (SA4) was probably produced by decompression melting of the kaersutite host.

Table 7. Representative electron microprobe analyses of silicate alteration (SA).

Megacryst	M2	M3	M1		M2	M3	M1			M1	M3			
Globule	f	f	c	e	d	f	d	e	f	f	b	b	c	d
Type	SA1		SA2				SA3			SA4				
Analysis#	6	7	8	9	10	11	12	13	14	15	16	17	18	19
SiO_2	48.19	41.16	44.32	42.64	36.77	41.79	26.24	21.71	25.51	29.70	25.38	30.58	33.14	29.46
TiO_2	0.09	0.08	0.02	0.05	0.07	0.29	0.43	0.10	0.15	5.71	5.86	5.41	5.77	6.25
Al_2O_3	14.44	13.46	39.25	37.89	22.72	24.66	22.06	19.15	20.15	10.57	6.92	7.60	8.86	10.92
Cr_2O_3	0.00	0.01	0.01	0.01	0.03	0.00	0.00	0.01	0.00	0.07	0.01	0.00	0.01	0.00
Fe_2O_3	0.74	0.74	3.71	3.71	4.49	7.77	33.53	41.96	29.00	13.94	19.96	14.20	14.03	16.72
MnO	0.06	0.00	0.04	0.04	0.00	0.00	0.04	0.07	0.04	0.41	0.26	0.08	0.13	0.19
MgO	19.02	17.59	0.65	5.65	15.65	1.80	0.57	0.70	0.53	6.33	7.28	6.79	7.02	7.70
NiO	0.04	0.01	0.20	0.09	0.14	0.00	0.00	0.03	0.52	0.24	0.00	0.02	0.06	0.00
CaO	1.37	1.17	1.53	0.84	1.48	1.94	1.16	2.54	2.86	11.30	12.21	14.17	14.56	12.99
Na_2O	0.06	0.04	0.17	0.28	0.08	0.07	0.05	0.33	0.64	0.17	1.14	1.49	1.50	0.99
K_2O	0.35	0.20	0.51	0.63	0.33	0.28	0.05	0.18	0.38	0.27	0.05	0.09	0.14	0.15
BaO	0.02	0.06	0.00	0.00	0.04	0.04	0.00	0.00	0.00	0.13	0.20	0.24	0.20	0.26
CoO	0.03	0.00	0.00	0.00	0.02	0.00	0.00	0.00	0.00	0.17	0.01	0.00	0.01	0.03
CuO	0.14	0.01	0.00	0.00	0.44	0.00	0.00	0.00	0.00	0.00	0.00	0.01	0.00	0.00
ZnO	0.00	0.00	0.00	0.00	0.07	0.00	0.00	0.00	0.00	0.02	0.04	0.06	0.11	0.22
SO_2	0.07	0.04	0.02	0.01	0.16	0.00	0.01	0.01	0.02	0.02	0.03	0.12	0.08	0.00
Total	84.61	74.57	90.43	91.84	82.50	78.65	84.14	86.85	79.80	79.04	79.35	80.85	85.61	85.87

At present there seems to be no way to derive the true composition of the original precursor of the IA and/or SA because of the observed variable alterations and variable phase compositions and ratios.

7. Conclusions

In this paper we describe different types of primary and secondary multiphase solid inclusions in ferrikaersutite megacrysts occurring in Quaternary alkali basalts from Dhanoon Volcano, Syria. The inclusion compositions reported include silicates, sulphides, oxides, Fe-rich- and/or silicate-alteration products.

Magnetite crystallised most probably from a Fe-rich melt in the early phases of inclusion growth. In a later phase, pyrrhotite, hematite, trevorite, and pseudobrookite crystallized.

Secondary inclusions were trapped along cracks in kaersutite after crystallizaton. Textures, solid mineral-chemistry as well as iron-rich and silicate alterations indicate that the original compositions of the inclusions phases were further modified by low-temperature post-magmatic deutric alteration of inclusion minerals. Late stage, near-surface alteration formed limonite and fine-grained sheet silicates possibly due to interaction with the last, H_2O-rich, melt and/or circulating fluids.

8. Acknowledgements

S. Nasir is indebted to the German Academic Exchange Service (DAAD) for financial support, which enabled his residence for two months at Universität Stuttgart. Thanks for Thomas Theye and H.-J. Massonne for their help with the electron microprobe analysis. The author is grateful to Martin Okrusch, Robert Stern and Ghaleb Jarar who made constructive suggestions to improve the manuscript. Thanks are also due to J. Touret for his help with finding fluid inclusions in polished section.

9. References

AL-MISHWAT, A., NASIR, S. 2003. Composition of the lower crust of the Arabian Plate: a xenolith perspective. *Lithos*, **72:** 45-72.

ALTHERR, R., HENJES-KUNST, F. and BAUMANN, A. 1990. Asthenosphere versus lithosphere as possible sources for basaltic magmas erupted during formation of the Red Sea: constraints from Sr, Rb and Nd isotopes. *Earth Plant. Sci. Lett.* **96:** 269-286.

ANDERSEN, T., NEUMAN, E.R. 2001. Fluid inclusions in mantle xenoliths. *Lithos* **55:** 299-318.

ANDERSEN, T., GRIFFIN, W.L. and O'REILLY, S.Y. 1987. Primary sulfide melt inclusions in mantle-derived megacrysts and pyroxenites. *Lithos,* **20:**279-294.

BOETTCHER, A, L. and O'NEIL, J.R. 1980. Stable isotope, chemical, and petrographic studies of high-pressure amphiboles and micas: evidence for metasomatism in the mantle source regions of alkali basalts and kimberlites. *Am. Jour. Sci*., **280(A):** 594-621.

CAMP, V.E. and ROOBOL, M.J. 1992. The Arabian continental alkali basalt province: part III. Evolution of the Harrat Kishb, Kingdom of Saudi Arabia. *Geol. Soc. Amer. Bull.* **104:** 379-396.

CHURIKOVA, T., WÖRNER, G., MIRONOV, N. and KRONZ, A. 2007. Volatile (S, Cl and F) and fluid mobile trace element compositions in melt inclusions: implications for variable fluid sources across the Kamchatka arc. *Contrib. Mineral. Petrol.* **154:** 217-239.

DWAIRI, I.M. 1998. Evaluation of Jordanian zeolite tuff as a controlled slow-release fertilizer for NH_4. *Envir. Geol*. **34:**1-4.

ERNST, W,G, and LIU, J. 1998. Experimental phase-equilibrium study of Al- and Ti-contents of calcic amphibole in MORB: A semiquantitative thermobarometer. *Am. Min.* **83:** 952-969.

FREZZOTTI, M.L. 2001. Silicate-melt inclusions in magmatic rocks: application to petrology. *Lithos* **55:** 273-299.

GUTMANN, J.T. 1974. Tubular voids within labradorite phenocrysts from Sonora, Mexico. *Am. Mineral*. **59:** 666-672.

HALTER, W.E, HEINRICH, C.A. and PETTKE, T. 2004a. Laser-ablation ICP-MS analysis of silicate and sulfide melt inclusions in an andesitic complex I: analytical approach and data evaluation. *Contrib. Mineral Petrol.* **147:** 385-396.

HALTER, W.E, HEINRICH, C.A. and PETTKE, T. 2004b. Laser-ablation ICP-MS analysis of silicate and sulfide melt inclusions in an andesitic complex II: evidence for magma mixing and magma chamber evolution. *Contrib. Mineral. Petrol*. **147:** 397-412.

HENJES-KUNST, F., ALTHERR, R. and BAUMANN, A. 1990. Evolution and composition of the lithospheric mantle underneath the western Arabian Peninsula: constraints from Sr-Nd isotope systematics of mantle xenoliths. *Contrib. Mineral. Petrol.* **105:** 406-427.

HONGFU, Z., NAKAMURA, E., JIN, Z. and AKIRA, I. 2006. Glass melt inclusion in clinopyroxene from Linqu Cenozoic basalt, Shandong Province, China. *Chinese Sci. Bull.* **21:** 1869-1876.

HOPS, J.J., GURNEY, J.J. and WINTERBURN, P. 1992. Megacrysts and high temperature nodules from the Jagersfontein kimberlite pipe. *Geol. Soc. Aust.* **14:** 759-770.

HURAI, V., SIMON, K., WIECHERT, U., HOEFS, J., KONECNY, P., HURAIVOA, M., PIRONON, J. and LIPKA, J. 1998. Immiscible separation of metalliferous Fe/Ti-oxide melts from fractionating alkali basalts: P-T-conditions and two-liquid elemental partitioning. *Contrib. Mineral. Petrol*. **133:** 12-29.

IBRAHIM, K., and HALL, A. 2004. The authigenic zeolites of the Aritayn Volcaniclastic Formation, north-east Jordan. *Mineral Deposita* **31:** 514-522.

ILANI, S., HARLAVAN, Y., TARAWNEH, K., RABBA, I., WEINBERGER. R., IBRAHIM, K., PELZ, S. and STEINITZ, G. 2001. New K-Ar ages of basalts from the Harrat Ash Shaam volcanic field in Jordan: implications for the span and duration of the upper mantle upwelling beneath the western Arabian plate. *Geology*, **29:** 171-174.

IONOV, D.A., GRIFFIN, W.L. and O'REILLY, S.Y. 1997. Volatile-bearing minerals and lithophile trace elements in the upper mantle. *Chem. Geol.* **141:** 153-184.

KRIENITZ, M-S., HAASE, KM., MEZGER, K., ECKARDT, V. and SHAIKH-MASHAIL, M.A. 2006. Magma genesis and crustal contamination of continental intraplate lavas in northwest Syria. *Contrib. Mineral. Petrol.* **151:** 698-716.

KULLERUD, G., YUND, R.A. and MOH, G. 1969. Phase relations in the Cu – Fe – S and Cu – Ni – S systems. Pp. 323-343 in: Magmatic Ore Deposits (HDB Wilson Editor) *Econ. Geol. Monogr.* **4:** 323-343.

LAROCQUE, A.C.L., STIMAC, J., KEIT, J.D. and HUMINICKY, M.A. 2000. Evidence for open- system behavior in immiscible Fe-S-O-liquids in silicate magmas: implications for contributions of metals and sulfur to ore-forming fluids. *Canad. Mineral*. **38:** 233-1249.

LAUBIER, M., SCHIANO, P., DOUCELANCE, R., OTTOLINI, L. and LAPORTE, D. 2007. Olivine- hosted melt inclusions and melting processes beneath the FAMOUS zone (Mid-Atlantic Ridge). *Chem. Geol.* **240:** 129-150.

LEAKE, BE and many others. 1997. Nomenclature of amphiboles: Report of the subcommittee on Amphiboles of the International Mineralogical Association Commission on New Minerals and Mineral Names. *Min. Mag.* **61:** 295-321.

LUSTRINO, M. and SHARKOV, E. 2006. Neogene volcanic activity of western Syria and its relationship with Arabian plate kinematics. *J Geol* **42:** 115-139.

MORIMOTO, N. and many others. 1988. Nomenclature of pyroxene. *Schweiz Mineral Petrog Mitt 68***:** 95-111.

MOUTY, M., DELALOYE, M., FONTIGNIE, D., PISKIN, O. and WAGNER, J.J. 1992. The volcanic activity in Syria and Lebanon between Jurassic and Actual. Schweiz *Mineral. Petrogr. Mitt.* **72:** 91-105.

NASIR, S. 1992. The lithosphere beneath the northwestern part of the Arabian plate (Jordan): evidence from xenoliths and geophysics. *Tectonophysics,* **201:** 357-370.

NASIR, S. 1994. Geochemistry and petrogenesis of Cenozoic volcanic rocks from the northwestern part of the Arabian ontinental alkali basalt province (Jordan). *African. Geosci . Rev.* **1:** 455-467.

NASIR, S. 1995. Cr-poor megacrysts from the Ash Sham volcanic field northwestern part of the Arabian plate. *J. Afr. Earth Sci.* **21:** 349-357.

NASIR, S. and MAHMOOD, S. 1991. Oxidation of olivine in lherzolitic xenoliths from NE- Jordan *Mu'tah J Research & Studies* **6:** 171-182.

NASIR, S. and SAFARJALANI, A. 2000. Lithospheric petrology beneath the northern part of the Arabian plate in Syria: evidence from xenoliths in alkali basalts. *J Afr Earth Sci* **30:** 149-168.

NASIR, S, AL-RAWAS, A. 2006. Mössbauer characterization of upper mantle ferrikaersutite. *Amer. Mineral*. **91:** 1163-1193.

NASIR, S., ABU-ALJARAYESH, I., MAHMOOD, S. and LEHLOOH, A. 1992. Oxidation state of the upper mantle beneath the northwestern part of the Arabian lithosphere. *Tectonophysics*, **213:** 359-366.

OBA, T. 1997. The stability fields of kaersutite and its substitution of $R^{2+} + 2Si = Ti + 2Al^{IV}$. Pp. 126-138 in *Synthetic and natural rock systems* (AKGupta, K Onuma, M Arima eds) Allied Publishers Ltd, Kolkata, India.

SHAW, J.E, BAKER, J.A, KENT, A.J.R., IBRAHIM, K.M. and MENZIES, M.A. 2007. The geochemistry of the Arabian lithospheric mantle – a source for intraplate volcanism. *J. Petrol*. **48:** 1495-1512.

STIMAC, J.A. and HICKMOTT, D. 1996. Ore partitioning in intermediate- to silicic magmas: PIXE results on natural mineral/melt assemblages. Pp. 197-235 in: *Giant Ore Deposits II: Controls on the Scale of Orogenic Magmatic-Hydrothermal Mineralization Proceeding* (A.H. Clark editor) Second Giant Ore Deposits Workshop (Kingston 1995).

TÖRÖK, K., BALI, E., SZABÓ, C. and SZAKAL, A. 2003. Sr-barite droplets associated with sulfide blebs in clinopyroxene megacrysts from basaltic tuff (Szentbekkalla: western Hungary). *Lithos*, **66:** 275-289.

WALLACE ,C. 1977. Anorthoclase-calcite rodding within kaersutite xenocryst from the Kakanui mineral breccia, New Zealand. *Am. Mineral*. **62:** 1038-1041.

ZAJACZ, Z., and SZABÓ, C. 2003. Origin of sulfide inclusions in cumulate xenoliths from Nograd-Gomor volcanic field Pannonian Basin (north Hungary/south Slovakia). *Chem. Geol.* **194:** 105-117.

Received 9 February 2009
Accepted 7 April 2009